Signatures of the fast dynamics in glassy polystyrene: first evidence by high-field Electron Paramagnetic Resonance of molecular guests

V.Bercu

Dipartimento di Fisica "Enrico Fermi", Università di Pisa, Largo B. Pontecorvo 3, I-56127 Pisa, Italy, Istituto per i processi Chimico-Fisici, via G.Moruzzi 1, I-56124 Pisa, Italy

M.Martinelli, C.A. Massa, L.A Pardi

IPCF-CNR, via G.Moruzzi 1, I-56124 Pisa, Italy

D.Leporini*

Dipartimento di Fisica "Enrico Fermi", Università di Pisa, and SOFT-INFM-CNR, Largo B. Pontecorvo 3, I-56127 Pisa, Italy

(Dated: August 30, 2005)

Abstract

The reorientation of one small paramagnetic molecule (spin probe) in glassy polystyrene (PS) is studied by high-field Electron Paramagnetic Resonance spectroscopy at two different Larmor frequencies (190 and 285 GHz). Two different regimes separated by a crossover region are evidenced. Below $180K$ the rotational times are nearly temperature-independent with no apparent distribution. In the temperature range $180 - 220K$ a large increase of the rotational mobility is observed with widening of the distribution of correlation times which exhibits two components: i) a delta-like, temperature-independent component representing the fraction of spin probes w which persist in the low-temperature dynamics; ii) a strongly temperature-dependent component, to be described by a power-distribution, representing the fraction of spin probes $1 - w$ undergoing activated motion over an exponential distribution of barrier heights $g(E)$. Above $180K$ a steep decrease of w is evidenced. The shape and the width of $g(E)$ do not differ from the reported ones for PS within the errors. For the first time the large increase of the rotational mobility of the spin probe at $180K$ is ascribed to the onset of the fast dynamics detected by neutron scattering at $T_f = 175 \pm 25K$.

PACS numbers: 64.70.Pf,76.30.-v,61.25.Hq

Keywords: fast motion, energy landscape, Electron Paramagnetic Resonance

I. INTRODUCTION

The study of glassy solid dynamics is a very active one[1,2]. Here, one is interested in the temperature range which is, on the one hand, well below the glass transition temperature T_g to neglect aging effect and consider the glassy system as one with constant structure and, on the other hand, high enough to neglect tunneling effects governing the low-temperature anomalies of glasses.

The fact that in the glassy state the structural relaxation comes to an halt on laboratory time scales does not imply that, however, that motion has ceased completely. In fact, even if no large-scale restructuring occurs, secondary processes are active. These includes the reorientation of side-groups[3,4], the most ubiquitous Johari-Goldstein β process[5] and possibly lower activation energy modes known as γ and δ relaxations[6]. Particular interest and a current subject of strong controversy is the so called fast dynamics of glasses, occurring in the time window $1-10^2$ ps with several studies carried out mainly by neutron[7–15] and Raman scattering[16–19] and numerical simulations[20]. It is observed that on heating in a temperature range below T_g the dynamics of glass-forming systems deviates from the harmonic behavior and quasielastic scattering starts to accumulate in the low frequency range of the scattering function $S(Q,\omega)$. Accordingly, the temperature dependence of the atomic mean-squared displacement also starts to deviate from the linear dependence. We will denote by T_f the onset temperature above which the deviation from the harmonic behavior becomes it apparent.

The microscopic origin of the fast dynamics is still a question open to a strong controversy. Correlations of T_f with the so-called Vogel-Fulcher temperature T_0 where the low-temperature extrapolation of the time scale of the α relaxation diverges have been noted[8,9]. However, cases with T_f well below[8,10,13] , equal[9,11], and well above[15] T_0 are reported. The role of carbon-carbon torsional barriers to drive the fast dynamics of glass-forming polymers was also pointed out[7]. In the particular case of polystyrene (PS) of interest here, T_f was found to be $175 \pm 25K$[12] and $200K$[10], i.e. well below $T_0 = 325K$. For PS the onset of the fast motion has been ascribed to the change of the *librational* dynamics of the side-chain phenyl ring[10,12] with expected involvement of the main-chain through the connecting bonds[14,21,22]. In fact, the phenyl rings in glassy PS undergo very complex 180° flips and librational motions[21,23] exploring several decades of characteristic times[22]. According

to Nuclear Magnetic Resonance (NMR) the flip motion becomes frozen at about $190K$[24,25].

In glasses the dynamics is thermally activated in the substructures of the minima of the energy landscape accounting for various subtle degrees of freedom[26]. Important information is conveyed by the energy barrier distribution $g(E)$ which in the glassy state is only weakly temperature-dependent[4,27]. For glassy PS this was tested by scaling light scattering data[28]. Buchenau confirmed that conclusion by comparing results from several techniques covering a wide time window from $1Hz$ up to about $100GHz$[29]. The same result has been reached by high-field Electron Paramagnetic Resonance (HF-EPR)[30]. The shape of the energy-barriers distribution $g(E)$ in glasses has been extensively investigated via experiments[2–4,18,27,28,30–35], theories[36–43] and simulations[44]. Basically, two different distributions are usually recovered, the gaussian distribution[2–4,18,27,33,36,38,44] and the exponential distribution[18,28,30,31,37,39–43]. The convolution of these two distributions[45] as well as the truncated Levy fligth, i.e. a power law with exponential cutoff, resembling the stretched exponential[35] were also considered.

It is interesting to relate $g(E)$ with the density of states, i.e.the distribution of the minima of the energy landscape. On the upper part of the landscape, being explored at high temperatures, the Central Limit theorem suggests that the density is gaussian[36,44]. At lower temperatures the state point is trapped in the deepest low-energy states which are expected to be exponentially distributed following general arguments on extreme-value statistics leading to the so-called Gumbel distribution[41]. Different models[36,42] and numerical simulations[43] support the conclusion. In particular, trap models suggest that $g(E)$ has the same shape of the exponential density of states[40,42] .

If the average trapping time τ before to overcome the barrier of height E at temperature T is governed by the Arrhenius law,

$$\tau = \tau_0 exp(E/kT) \tag{1}$$

k being the Boltzmann's constant, the distribution of barrier heights induces a distribution of trapping times $\rho(\tau)$. The explicit form of $\rho(\tau)$ for a gaussian distribution of barrier heights with width σ_E is the log-gauss distribution (LGD)

$$\rho_{LGD}(\tau) = \frac{1}{\sqrt{2\pi\sigma^2}} \exp\left[-\frac{1}{2\sigma^2}\left(\ln\frac{\tau}{\tau_{LGD}}\right)^2\right]\frac{1}{\tau} \tag{2}$$

$\sigma = \sigma_E/kT$ is the width parameter. If the distribution of barrier heights is exponential with width $\overline{E}$

$$g(E) = \begin{cases} 0 & \text{if } E < E_{min} \\ \frac{1}{\overline{E}} exp(-\frac{E-E_{min}}{\overline{E}}) & \text{if } E \geq E_{min} \end{cases} \tag{3}$$

$\rho(\tau)$ is expressed by the power-law distribution (PD)

$$\rho_{PD}(\tau) = \begin{cases} 0 & \text{if } \tau < \tau_{PD} \\ x\tau_{PD}^{x}\tau^{-(x+1)} & \text{if } \tau \geq \tau_{PD} \end{cases} \tag{4}$$

with $x = kT/\overline{E}$ and $\tau_{PD} = \tau_0\, exp(E_{min}/kT)$. Note that the absence of energy barriers below E_{min} does not change the shape of ρ_{PD} and allows for the temperature dependence of τ_{PD}.

If the width of the energy-barriers distribution is vanishingly small, a single trapping time (SCT) is found with:

$$\rho_{SCT}(\tau) = \delta(\tau - \tau_{SCT}) \tag{5}$$

The use of suitable probes to investigate the secondary relaxations in glasses by NMR[2,3,25,32,45,46], EPR[47–50] and Phosphorescence[51] studies is well documented. In spite of that efforts, the relation between the probe motion and the host dynamics is usually not obvious with few exceptions which notably involves small molecules[25,30,46,48–50]. It was also noted that small molecules, e.g. xanthone and benzophenone, are more sensitive to shorter segmental motions occurring at lower temperatures[51].

During the last few years continuous-wave (CW) and pulsed HF-EPR techniques were developed involving large polarizing magnetic fields, e.g. $B_0 \cong 3T$ corresponding to Larmor frequencies about $95GHz$ (W band),[52,53] or even larger frequencies[30,54,55]. HF-EPR is widely used in solid-state physics[56–58], biology[59–63] and polymer science[30,64–67]. One major feature is the remarkable orientation resolution[67] due to increased magnitude of the anisotropic Zeeman interaction leading to a wider distribution of resonance frequencies[68,69]. Recently, HF-EPR studies evidenced the exponential distribution of the energy barriers of the deep structure of the energy landscape in glassy PS[30] at $240K$ and $270K$.

In the present paper we present a detailed temperature study of the reorientation of a small probe molecule in glassy PS. The results extend the findings of ref.[30]. Moreover,

evidence is presented of a remarkable change of the rotational dynamics at $\cong 200K$ which is interpreted as clear signature of the onset of fast dynamics of glassy PS.

The paper is organized as follows. In Sec. II the necessary background on EPR spectroscopy is briefly outlined. In Sec.III experimental details are given. In Sec. IV the results are presented and discussed. The conclusions are summarized in Sec.V.

II. EPR BACKGROUND

A. Lineshape

The EPR signal is detected in paramagnetic systems. Since most polymers are diamagnetic, paramagnetic probe molecules (spin probes) are usually dissolved in them. The main broadening mechanism of the EPR line shape of the spin probe is determined by the coupling between the reorientation of the latter and the relaxation of the electron magnetization $\mathbf{M}$ via the anisotropy of the Zeeman and the hyperfine magnetic interactions. When the molecule rotates, the coupling gives rise to fluctuating magnetic fields acting on the spin system. The resulting phase shifts and transitions relax the magnetization and broadens the resonance[68,69]. One important parameter to describe the rotational dynamics of the spin probe is the correlation time τ_l, i.e. the area below the correlation function of the spherical harmonic $Y_{l,0}$.

The occurrence of a static distribution of correlation times in glasses leads to evaluate the EPR line shape $L(B_0)$, which is usually detected by sweeping the static magnetic field B_0 and displaying the first derivative, as a weighted superposition of different contributions:

$$L(B_0) = \int_0^\infty d\tau_2 L(B_0, \tau_2)\ \rho(\tau_2) \tag{6}$$

where $L(B_0, \tau_2)$ is the EPR line shape of the spin probes with correlation time τ_2 and $\rho(\tau_2)$ is the τ_2 distribution. The choice of labeling the different contributions by τ_2 is arbitrary. An efficient numerical method to calculate the HF-EPR line shape is detailed elsewhere[65].

B. Model of the rotational motion

Because of the roughness of the energy landscape and the highly branched character of the free volume distribution, one expects that small spin probes undergo jump dynamics in glasses[48,70,71]. In the presence of jumps correlations are lost roughly after one single trapping time, i.e. $\tau_l \cong \tau$. For $l = 2$ a simple rotational jump model yields[48]

$$\tau_2 = \frac{\tau^*}{\left[1 - \frac{\sin\left(\frac{5\phi}{2}\right)}{5\sin\left(\frac{\phi}{2}\right)}\right]} \tag{7}$$

where ϕ and τ^* are the size of the angular jump and the mean residence (trapping) time before a jump takes place, respectively. In the limit $\phi << 1$ eq.7 reduces to $\tau_2 = 1/6D = \tau^*/\phi^2$, where D is the rotational diffusion coefficient, i.e. the isotropic diffusion model. If $\phi \cong 1$, $\tau_2 \cong \tau^*$. Similar conclusions are drawn for arbitrary l values. The above discussion suggests that in the presence of jump dynamics the distribution of the rotational correlation times τ_l and the distribution of trapping times τ of the spin probe do not differ too much. Henceforth, to emphasize that viewpoint, τ_2 will be denoted as τ.

The identification of the rotational correlation time with the waiting time before one activated jump takes place, is questionable when the latter becomes extremely rare. In fact, if energy barriers are too high, entropic-like, alternative pathways may become competitive to cancel the orientation correlations. A simple account of that is provided by the truncation of $\rho(\tau)$ in eq.6 beyond a certain τ_{max} to give an effective distribution

$$\rho_T(\tau) = H(\tau_{max} - \tau)\rho(\tau) + w\delta(\tau - \tau_{max}) \tag{8}$$

where $\delta(x)$ is the Dirac delta, $H(x) = 1$ for $x > 0$ and zero otherwise and

$$w = \int_{\tau_{max}}^{\infty} d\tau\ \rho(\tau) \tag{9}$$

The weight w is the fraction of *trapped* molecules, i.e. the ones losing the rotational correlations by undergoing not-activated motion. Note that for consistence to hold τ_{max} must be nearly temperature-independent. Henceforth, ρ_{TPD} will denote ρ_T in the particular case $\rho = \rho_{PD}$, eq.4 with $\tau_{PD} < \tau_{max}$. Representative plots of the bimodal distribution ρ_{TPD} are shown in fig.1.

C. Adjustable parameters

The data analysis fits the experimental HF-EPR lineshapes collected at different temperatures and different operating frequencies (in the present case $190\,GHz$ and $285\,GHz$) with the theoretical prediction as expressed via eq.6 and the proper distribution function ρ_T, eq.8. It is worthwhile to state explicitely the number of adjustable parameters. They are divided in two sets:

i) the parameters which are temperature- and frequency- independent. The set includes the six magnetic parameters of the spin probe (the principal components of the g and hyperfine tensors) and the jump angle ϕ;

ii) the parameters which are temperature-dependent and almost frequency-independent. The set includes the width of the energy-barrier distribution, e.g. $\overline{E}$ for the exponential distribution, eq.3, and the characteristic time scales of ρ_T, eq.8. In the case $\rho_T = \rho_{TPD}$, they are the shortest and the longest correlation time τ_{PD} and τ_{max} respectively. Having set the former time scales the weight w is not adjustable. In the simplest case of no distribution of correlation times (eq.5) τ_{SCT} only is adjusted

D. Features of the HF-EPR lineshape

The change of the rotational rates of the spin probe results in marked effects on the HF-EPR lineshape for correlation times in the range of few picoseconds up to hundreds of nanoseconds. Examples are drawn in fig.2 at $190GHz$ for two different jump angles and the SCT model eq.5. For fast reorientation the anisotropy of the magnetic interactions is effectively averaged, and a triplet of narrow lines is observed (lineshape a). For slower reorientation rates the triplet structure is lost (lineshapes b, c). No appreciable dependence on the jump angle is observed here. When the reorientation rate decreases further, the anisotropy of the Zeeman and hyperfine tensors is no longer averaged and the spectrum becomes significantly broader.

In this regime with correlation times roughly $1-10ns$ the line shape is highly sensitive to the specifics of the reorientation process and its rate (lineshapes $d-g$). As an elementary tool to appreciate the sensitivity the distance between the outermost peaks of the lineshape ΔB is used (see Fig.2). The dependence of ΔB on the reorientation rate for small and large

jump angles is presented in Fig.3 . It is clearly seen that in the presence of diffusive motion (small ϕ values) ΔB changes of about $7mT$ (about 25%) when the correlation time change of a factor of about 50. Given the accuracy of the measurement of ΔB in the experiment (about $0.1mT$), similar changes are quite large. Differently, for large jump angles ΔB is weakly dependent on the reorientation rate even if the changes are still experimentally detectable.

III. EXPERIMENTAL DETAILS

PS was obtained from Aldrich and used as received. The weight-average molecular weight is M_w=230 kg mol^{-1}, polydispersity $M_w/M_n = 1.64$ and T$_g$=367 K. The free radical used as spin probe was 2,2,6,6-tetramethyl-1-piperidinyloxy (TEMPO) from Aldrich. TEMPO has one unpaired electron spin S=1/2 subject to hyperfine interaction with the nitrogen nucleus with spin I=1. The chemical structures of PS and TEMPO are shown in fig.4. Notice that TEMPO and the phenyl group of PS have similar shape. TEMPO is stiff with almost spherical shape[50]. It has an average van der Waals radius $r_{TEMPO} = 3.3 \pm 0.2\mathring{A}$ and may be sketched as an oblate ellipsoid with semiaxes $r_{||} \sim 2.7\mathring{A}$ and $r_{\perp} \sim 3.7\mathring{A}$. The sample was prepared by the solution method[72] by dissolving TEMPO and PS in chloroform. The solution was transferred onto the surface of a glass slide and heated at $T_g + 10K$ for 24 h. After that procedure no chloroform was detected by NMR. The sample of about 0.8 cm^3 was placed in a Teflon sample holder in a single-pass probe cell. The spin probe was less then 0.08% in weight, thus resulting in a extremely limited influence on PS. Appreciable broadening of the EPR line shape due to the spin-spin interaction is observed for concentrations larger than 0.2% in weight. No segregation of the spin probe was evidenced. Samples aged at room temperature for six months exibited no apreciable change of the EPR line shape. The EPR experiments were carried out on the ultrawide-band EPR spectrometer which is detailed elsewhere[73]. The investigated temperatures are $50K, 180K, 200K, 220K, 240K, 270K$. The used frequencies of the spectrometer are $190GHz$ and $285GHz$. The multi frequency approach ensures better accuracy for determining the spin probe dynamics. All spectra were recorded and stored in a computer for off-line analysis. Magnetic parameters of TEMPO are drawn from the best-fit values at $50K$ and listed in fig.2.

IV. RESULTS AND DISCUSSION

Fig. 5 shows the temperature dependence of the distance ΔB at $190GHz$ and $285GHz$ (see fig.2 for the definition). The evidence that ΔB is still changing at temperatures as low as $50K$ proves that the reorientation motion of TEMPO is detectable even at such low temperatures. Moreover, the changes of ΔB with the temperature and then with TEMPO reorientation rate rules out, according to fig.3, that TEMPO proceeds by wide angular jumps. Fig. 5 also shows the temperature dependence of the average linewidth of the three high-field lines of the HF-EPR lineshape (see fig.2). Noticeably, it approaches a plateau value below $180K$ signaling minor sensitivity on the TEMPO reorientation.

A. Low temperature regime: $T \leq 180K$

Fig. 6 shows the lineshape at $190GHz$ and $285GHz$ of TEMPO in PS at $50K$. It is seen that the lineshapes at two different frequencies are well fitted by a *single* correlation time (SCT model, eq.5, two adjustable parameters, τ_{SCT}, ϕ and a single set of magnetic parameters). The small discrepancy between the simulation and the peak at low magnetic field was already noted[74]. At such very slow reorientation rates the lineshape is weakly sensitive to the jump size. In fact, the quality of the fit does not change if the jump angle ϕ spans the range $20° - 60°$.

Fig. 7 shows the lineshape at $190GHz$ and $285GHz$ of TEMPO in PS at $T = 180K$. Again, the SCT model provides good fits even if discrepancies are larger than at $50K$. The faster rotational rate allows for better definition on the jump angle ϕ whose best-fit value is in the range $20° - 35°$.

B. Crossover regime: $T \cong 200K$

Fig. 8 shows the lineshape at $190GHz$ and $285GHz$ of TEMPO in PS at $T = 200K$. Here, the best-fit curve by using the SCT model deviates from the experiment. Better agreement is provided by considering the truncated power distribution of correlation times ρ_{TPD} (eq.8 with $\rho = \rho_{PD}$, eq.4). That choice is guided by the attempt to bridge the low temperature regime with the high temperature one ($T \geq 220K$, see Sec.IV C) where TEMPO was reported to exhibit unambiguously a power distribution of correlation times[30]. $\rho_{TPD}(\tau)$ is

truncated for $\tau > \tau_{max}$, τ_{max} being the rotational correlation time of trapped TEMPO (Sec.II B). It is expected to be weakly temperature-dependent. From this respect, it is natural to identify τ_{max} with τ_{SCT} at $180K$, i.e. to assume that the rotational dynamics of TEMPO at $T \leq 180K$ is a non-activated process (in fact τ_{SCT} between $50K$ and $180K$ is found almost temperature-independent, see figs.6,7). That constraint was kept for all the temperatures $T \geq 200K$. i.e. all the simulations in terms of ρ_{TPD} set τ_{max} at the best-fit values of τ_{SCT} at $180K$ with $\phi = 20°$ which is the best-fit value of the jump angle for both frequencies in that temperature range. Due to this strategy, $\rho_{TPD}(\tau)$ has the same adjustable parameters of $\rho_{PD}(\tau)$ eq.4 which, in turn, adds only *one* adjustable parameter to the one of the elementary SCT model, eq.5. Two relevant outcomes of the TPD distribution are the quantities w, eq.9 , and $\overline{E}$ which express the fraction of trapped TEMPO molecules and the width of the energy-barrier distribution, respectively. At $200K$ $w_{190GHz} = 0.44$ and $w_{285GHz} = 0.34$. The complete temperature dependence of w and $\overline{E}$ will be presented in the next section.

A consistency check of the implementation of the TPD model at $T \geq 200K$ is to compare the best-fits of the EPR lineshape at $180K$ by the SCT and TPD models. One notices that the best-fit value τ_{PD} is within the errors (see fig. 12) equal to τ_{SCT}, i.e. the untrapped TEMPO fraction is negligible. This is understood by noting that at $180K$ the TPD model adds with respect to the SCT model a power distribution of correlation times which are shorter than the single correlation time τ_{SCT}. If the shortest correlation time τ_{PD} differs too much from the longest one τ_{SCT}, the distance between the outermost peaks of the lineshape ΔB (see fig. 2) decreases and the agreement between the theoretical and the experimental curves worsens.

C. High temperature regime: $T \geq 220K$

At higher temperatures the agreement of the TPD model with the experiment becomes more pronounced. In particular, on increasing the temperature, the fraction of trapped TEMPO molecules w decreases markedly (fig.9), making the differences between TPD and PD models, eq.4, immaterial. In fact, a multiple frequency HF-EPR study of TEMPO in PS at $240K$ and $270K$ reported clear evidence of power distribution of correlation times

$\rho_{PD}(\tau)$[30]. For illustration fig. 10 presents part of that results obtained at 190 GHz and 270 K. It compares the best-fit of the lineshape by the SCT model (eq.5, two adjustable parameters: τ_{SCT}, ϕ), the LGD model (eq.2, three adjustable parameters: τ_{LGD}, ϕ and σ) and the PD model (eq.4, three adjustable parameters: τ_{PD}, ϕ and x). After adjustment, it was found that the best-fit value of the jump angle for the three models was the same, i.e. $\phi = 20°$. The better agreement by using ρ_{PD} is apparent.

Fig.11 presents the temperature dependence of the width of the energy-barrier distribution $\overline{E}$ as drawn by best-fit procedure of the HF-EPR lineshapes at $190GHz$ and $285GHz$ in terms of the TPD model. To get that results, the parameters $x = kT/\overline{E}$, and τ_{PD} of eq.4 only were adjusted with constant jump angle $\phi = 20°$. The lowest temperature of the plot is $200K$, below which TEMPO is trapped ($w \cong 1$, fig.9) and then unable to probe the energy-barrier distribution. It is noted that $\overline{E}$ is temperature-independent in the range $200 - 240K$. It is interesting to compare the exponential energy-barrier distribution which is experienced by TEMPO, $g(E)$, and $g_{PS}(E)$, i.e. the exponential distribution of barrier-heights of PS which was evidenced by internal friction[31], Raman[18] and light scattering[28]. The measured widths were $\overline{E}_{IF}/k = 760 \pm 40K$, $\overline{E}_{Raman}/k = 530 \pm 60K$ and $\overline{E}_{LS}/k = 530 \pm 40K$, respectively. By comparison, it is seen that the distribution of energy barriers $g(E)$ probed by TEMPO has not only the same shape of the PS one, but it exhibits also comparable width. In particular, the constancy of $\overline{E}$ for TEMPO at low temperatures is consistent with the conclusion that the latter probes the barrier-height distribution of glassy PS which is expectedly temperature-independent[4,27]. The apparent decrease of $\overline{E}$ at the highest temperature is, most probably, not due to PS which is still well below T_g but to faster reorientation of TEMPO leading to a decoupling from PS dynamics.

It was noted that both the shape and the width of $g_{PS}(E)$ manifest within the errors weak frequency-dependence in the wide range covered by the slow mechanic measurements carried out between $1Hz - 87KHz$ and the fast Raman and light scattering measurements data ($\sim 3 - 300GHz$)[29]. The HF-EPR measurements at 180 and $285GHz$ confirm that invariance if one assumes $g(E) \cong g_{PS}(E)$.

D. Characteristic times of TEMPO in PS

Fig.12 presents the overall temperature dependence of the characteristic times describing the reorientation of TEMPO according to the SCT (eq.5, τ_{SCT}) , PD (eq.4, τ_{PD}) and TPD (eq.8 with $\rho = \rho_{PD}$, τ_{PD} and τ_{max}) models. On heating, after a flat region between $50 - 180K$ where TEMPO exhibits a single correlation time τ_{SCT}, between $180 - 220K$ a second component of the distribution of correlation times arises, being described by a truncated power distribution of correlation times whose shortest timescale τ_{PD} drops of a factor of about 80. The increase of the rotational mobility parallels the strong decrease of the fraction of trapped TEMPO molecules w, fig.9. The changes of the bimodal distribution of correlation times by decreasing w is pictured by fig.1. Interestingly, similar effects on guest molecules were reported. NMR showed that toluene (similar in shape to TEMPO, see fig.4) in glassy PS exhibits both frozen and mobile components, the latter arising at about $170 - 180K$ (after corrections for the PS plasticization due to the not small toluene concentration)[25,46]. Moreover, it was noted by EPR that oriented spin probes in PS lose their alignment above $\cong 200K$[47]. **It is worthwhile that the change of the rotational dynamics of TEMPO in PS around** $200K$ **cannot be ascribed in an obvious way to changes in the free-volume where TEMPO is accomodated, as in other cases[50]. This follows from the study of the unoccupied volume of PS by the positron annihilation technique[75]. It was found that the lifetime of ortho-positronium, which is related to the free-volume size[50,75], increases smoothly with trivial linear temperature-dependence in the range** $30 - 260K$**.**

We intepret the increased rotational mobility of TEMPO above $180K$ as a signature of the onset of the fast dynamics of PS which, according to neutron scattering studies is located at $T_f = 175 \pm 25K$[10,12]. In fact, our results suggest the following scenario (see fig.13). Below $180K$ TEMPO molecules are unable to hop over barriers. The orientation correlations are lost by non-activated entropic-like processes with negligible distribution of the characteristic timescales. Above that temperature the onset of fast PS dynamics, which is well coupled to the rotational timescales of TEMPO, facilitate the crossover of the barriers which is successfully accomplished by a fraction $(1 - w)$ of TEMPO molecules. Jumping over the barriers allows TEMPO to probe the exponential distribution of PS barrier-heights. As a consequence, a distribution of correlation times arises.

The onset of fast dynamics has been ascribed to the change of the *librational* dynamics of the side-chain phenyl ring[10,12]. In fact, according to NMR the flip motion of the ring becomes frozen at about $190K$[24,25]. Thus, it is tempting to conclude that the detrapping of TEMPO above $180K$ is due to the onset of some motion of the phenyl ring which is expectedly well coupled to TEMPO due to the similar shape (see fig.2). However, the role of carbon-carbon torsional barriers to drive the fast dynamics of glass-forming polymers was also pointed out[7]. Additional work is needed to discriminate between these two views.

As to the region $T \geq 220K$ the Arrhenius fit of the temperature dependence of τ_{PD} yields $\tau_0 = 90ps, E_{min} = 0.5KCal/mol$ at $190GHz$ and $\tau_0 = 20ps, E_{min} = 1KCal/mol$ at $285GHz$, where E_{min} is interpreted as the minimum barrier-height of the exponential distribution seen by TEMPO (see eq.3).

Since the longest correlation time of TEMPO which is made accessible by HF-ESR is $\tau^* \sim 100ns$, one wonders if the energy-barrier distribution $g(E)$ is characterized over a meaningful range. From eq.1 one estimates the maximum energy barrier which TEMPO may overcome leading to appreciable motional narrowing of the lineshape as $E_{max} \sim kT\ ln(\tau^*/\tau_0)$. In the worst case ($T = 220K$) $E_{max}/k \sim 2000K \gtrsim (E_{min} + 2\overline{E})/k$, i.e. TEMPO probes a wide portion of the overall range of the energy barriers. At $270K$ the situation is even more favourable[30].

V. CONCLUSIONS

The study of the reorientation of the small and nearly spherical guest molecule TEMPO in PS by HF-EPR evidences two different regimes separated by a crossover region. Below $180K$ the rotational times are nearly temperature-independent with no apparent distribution. In the temperature range $180-220K$ a large increase of the rotational mobility is observed with widening of the distribution of correlation times which may be divided in two components: i) a delta-like, temperature-independent component representing the fraction of TEMPO molecules w which persist in the low-temperature dynamics, namely they lose their rotational correlations *before* a jump over barriers takes place; ii) a strongly temperature-dependent component to be described by a power-distribution representing the fraction of TEMPO molecules $1 - w$ undergoing activated motion over an exponential distribution of barrier heights $g(E)$. Above $220K$ w is negligibly small. The pictorial view of the above scenario

is given in fig.13. The exponential shape of $g(E)$ was evidenced also by other studies on PS[18,28,31] which reported widths $\overline{E}$ in the range of the one exhibited by TEMPO. The finding that the deep structure of the energy landscape of PS exhibits an exponential energy-barriers distribution agrees with results from extreme-value statistics[41] and the trap model by Bouchaud and coworkers[40,42]. The change of the rotational dynamics of TEMPO in PS around $200K$ cannot be ascribed in an obvious way to changes in the free-volume where TEMPO is accomodated. Instead, the onset of the large increase of the rotational mobility of TEMPO at $180K$ is interpreted as signature of the onset of the fast motion which was detected by neutron scattering at $175 \pm 25K$[10,12] and ascribed either to the change of the *librational* dynamics of the side-chain phenyl ring of PS[10,12] or the carbon-carbon torsional barriers[7].

Acknowledgments

J.Colmenero and A.P.Sokolov are gratefully acknowledged for helpful discussions.

---

* Electronic address: `dino.leporini@df.unipi.it`

[1] C. A.Angell, K. L.Ngai, G. B. McKenna, P. F.McMillan, S. W. Martin, J. Appl. Phys. **88**, 3113 (2000).

[2] R. Böhmer , G.Diezemann , G.Hinze , E.Rössler , Prog.Nucl.Mag.Reson. **39**, 191 (2001).

[3] F.Qi, R.Böhmer, H.Sillescu, Phys.Chem.Chem.Phis.**3**, 4022 (2001).

[4] L. Wu, Phys.Rev.B **43**, 9906 (1991).

[5] G. P.Johari, M.Goldstein, J.Chem.Phys. **53**, 2372 (1970).

[6] N.G. McCrum, B.E.Read , G.Williams, *Anelastic and Dielectric Effects in Polymeric Solids* (Wiley, New York, 1967).

[7] J.Colmenero, A.Arbe, Phys.Rev.B **57**, 13508 (1998).

[8] G. Floudas, J. S. Higgins, F. Kremer, and E. W. Fischer, Macromolecules **25**, 4955 (1992).

[9] T.Kanaya, K.Kaji, Adv.Polym.Sci. **154**, 87 (2001).

[10] T.Kanaya, T.Kawaguchi,K.Kaji, J.Chem.Phys. **104**, 3841 (1996).

[11] T. Kanaya, K.Kaji, J.Bartos, M.Klimova, Macromolecules **30** 1107 (1997).

[12] B. Frick, U. Buchenau, and D. Richter, Colloid Polym. Sci. **273**, 413 (1995).

[13] U. Buchenau, C. Schnfeld, D. Richter, T. Kanaya, K. Kaji, and R. Wehrmann, Phys. Rev. Lett. **73**, 2344 (1994).

[14] U. Buchenau, C.Pecharroman, R.Zorn, B.Frick, Phys. Rev. Lett. **77**, 659 (1996).

[15] B.Frick, D. Richter, Phys.Rev.B **47**, 14795 (1993).

[16] Y.Ding, V.N.Novikov, A.P.Sokolov, A.Cailliaux, C.Dalle-Ferrier, C.Alba-Simionesco, B.Frick, Macromolecules **37**, 9264 (2004).

[17] V.N.Novikov, A.P.Sokolov, B.Strube, N.V.Surovtsev, E.Duval, A.Mermet, J.Chem.Phys. **107**, 1057 (1997).

[18] A.P.Sokolov, V.N.Novikov, B.Strube, Europhys.Lett. **38**, 49 (1997).

[19] A.P.Sokolov, U. Buchenau, W.Steffen, B.Frick, A.Wischnewski, Phys.Rev.B **52**, R9815 (1995).

[20] R.J.Roe, J.Non-Cryst. Solids **235-237**, 308 (1998).

[21] J.Schaefer, M.D.Sefcik,E.O.Stejskal,R.A.McKay, Macromolecules **17**,1107 (1984).

[22] R.Khare, M.E.Paulaitis, Macromolecules **28**,4495 (1995).

[23] H.W.Spiess, Colloid Polym.Sci., **261**, 193 (1983).

[24] E.Rössler, Dissertation, Universität Mainz, 1984.

[25] H.Sillescu, Makromol. Chem., Macromol. Symp. **1** , 39 (1986).

[26] C.A. Angell, Nature **393**, 521 (1998).

[27] L.Wu, S.R.Nagel, Phys.Rev.B **46**, 11198 (1992).

[28] N.V.Surovtsev, J.A.H.Wiedersich, V.N.Novikov, E.Rössler, A.P.Sokolov, Phys.Rev.B **58**, 14888 (1998).

[29] U.Buchenau, Phys.Rev.B **63** 104203 (2001).

[30] V Bercu, M Martinelli, C AMassa, L A Pardi, D.Leporini, J. Phys.: Condens. Matter **16** L479 (2004).

[31] K.A.Topp, D.G.Cahill, Z.Phys.B **101**,235 (1996).

[32] E.Rössler, M.Taupitz, K.Börner, M.Schulz, H.M.Vieth, J.Chem.Phys. **92**, 5847 (1990).

[33] M.Vogel, E.Rössler, J.Chem.Phys. **114**, 5802 (2001).

[34] M.Vogel, E.Rössler, J.Chem.Phys. **115**, 10883 (2001).

[35] N.T.Gorham, R.C.Woodward, T.G.St.Pierre, R.L.Stamps, M.J.Walker, D.Greig, J.A.D.Matthew, J.Apll.Phys. **95**, 6983 (2004).

[36] B.Derrida, Phys.Rev.B **24**, 2613 (1981).

[37] H.Scher,E.W.Montroll, Phys.Rev.B **12**, 2455 (1975).

[38] H.Bässler, Phys.Rev.Lett.**58**, 767 (1987).

[39] T.Odagaki, Phys.Rev.Lett. **75**,3701 (1995).

[40] C.Monthus, J -P.Bouchaud, J.Phys.A: Math.Gen. **29**, 3847 (1996).

[41] J -P.Bouchaud, M.Mezard, J.Phys.A: Math.Gen. **30**, 7997 (1997).

[42] B.Rinn, P.Maass, J -P.Bouchaud, Phys.Rev.B **64**, 104417 (2001).

[43] J.C.Schön, P.Sibani, Europhys.Lett. **49**, 196 (2000).

[44] R.A.Denny, D.R.Reichman, J -P Bouchaud, Phys.Rev.Lett. **90**, 025503 (2003).

[45] E.Rössler, M.Taupitz, H.M.Vieth, J.Phys.Chem. **94**, 6879 (1990).

[46] E.Rössler, H.Sillescu, H.W.Spiess, Polymer **26**,203 (1985).

[47] A.Kh.Vorobiev, V.S.Gurman, T.Klimenko, Phys.Chem.Chem.Phys. **2**, 379 (2000).

[48] L.Andreozzi, F.Cianflone, C.Donati, D.Leporini, J.Phys.: Condens.Matter **8**, 3795 (1996).

[49] M.Faetti, M.Giordano, D.Leporini, L.Pardi, Macromolecules **32**, 1876 (1999).

[50] A.Barbieri, G.Gorini, D.Leporini, Phys. Rev. E **69**, 061509 (2004).

[51] M.Christoff, T.D.Z.Atvars, Macromolecules **32**, 6093 (1999).

[52] M.A.Ondar, O.Y.Grinberg, L.G.Oranskii, V.I.Kurochkin, Y.L.Lebedev, J. Struct. Chem. **22**, 626 (1981).

[53] D.E.Budil, K.A.Earle, J.H.Freed, J. Phys. Chem. **97**, 1294 (1993).

[54] T.N. Makarov, A.N. Savitsky, K.Mobius, D.Beckert, H.Paul, J.Phys,Chem. A **109**, 2254 (2005).

[55] H.Blok, J.A.J.M.Disselhorst, S.B.Orlinskii, J.Schmidt, J.Mag.Reson. **166**, 92 (2004).

[56] M.Martinelli, C.A.Massa, L.A.Pardi,V.Bercu, F.F.Popescu, Phys. Rev. B **67**, 014425 (2003).

[57] A.Rockenbauer, G.Csanyi, F.Fulop, S.Garaj, L.Korecz, R.Lukacs, F.Simon, L.Forro, S.Pekker, A.Janossy, Phys.Rev.Lett. **94**, 066603 (2005).

[58] S.B. Orlinskii, J.Schmidt, P.G.Baranov, D.M.Hofmann, C.D.Donega, A.Meijerink, Phys.Rev.Lett. **92**, 047603 (2004).

[59] Z.C.Liang, J.H.Freed, J. Phys. Chem. B **103**, 6384 (1999).

[60] Z.C.Liang, J.H.Freed, R.S.Keyes, A.M.Bobst, J. Phys. Chem. B **104**, 5373 (2000).

[61] P.P.Borbat, A.J.Costa-Filho, K.A.Earle, J.K.Moscicki, J.H.Freed, Science **291**, 266 (2001).

[62] M.R.Fuchs, E.Schleicher, A.Schnegg,C.W.M.Kay, J.T.Torring, R.Bittl, A.Bacher, G.Richter, K.Mobius, S.Weber, J. Phys. Chem. B **106**, 8885 (2002).

[63] K.O.Schafer, R.Bittl, F.Lendzian, V.Barynin, T.Weyhermuller, K.Wieghardt, W.Lubitz, J.

Phys. Chem. B **107**, 1242 (2003).

[64] J.Pilar, J.Labsky, A.Marek, D.E.Budil, K.A.Earle, J.H.Freed, Macromolecules **32**, 4438 (2000).

[65] D.Leporini, X.X.Zhu, M.Krause, G.Jeschke, H.W.Spiess, Macromolecules **35**, 3977 (2002).

[66] D.Leporini, V.Schädler, U.Wiesner, H.W.Spiess, G.Jeschke, J. of Non-Crystalline Solids **307310**, 510 (2002).

[67] D.Leporini, V.Schädler, U.Wiesner, H.W.Spiess, G.Jeschke, J.Chem.Phys. **119**, 11829 (2003).

[68] *Spin labeling: Theory and Applications*,edited by L.J. Berliner (Academic, New York, 1976); *Biological magnetic resonance*, edited by L.J.Berliner and J. Reuben (Plenum, New York,1989), Vol 8.

[69] L.T.Muus and P.W.Atkins Electron spin relaxation in liquids (New York, Plenum, 1972).

[70] J. Kim, T. Keyes, J.Chem.Phys. **121**, 4237 (2004).

[71] C. De Michele, D. Leporini, Phys. Rev. E **63**, 036702 (2001).

[72] J.W.Saalmueller, H.W.Long, T.Volkmer, U.Wiesner, G.G.Maresch, H.W.Spiess, J.Polym. Sci.: Part B: Polymer Physics **34**, 1019 (1996).

[73] G.Annino, M.Cassettari, M.Fittipaldi, L.Lenci, I.Longo, M.Martinelli, C.A.Massa and L.A.Pardi, Appl.Magn.Reson.**19**, 495 (2000).

[74] D.E.Budil, K.A.Earle and J.H.Freed, J.Phys.Chem. **97**, 1294 (1993).

[75] A. Uedono, T. Kawano, S. Tanigawa, M. Ban, M. Kyoto, T. Uozumi, J.Polym. Sci.: Part B: Polymer Physics **34**, 2145 (1996).

Figure captions

FIG. 1: Schematic view of the bimodal distribution of correlation times ρ_{TPD} (eq.8 with $\rho = \rho_{PD}$) for different values of the trapped fraction w. $\tau_{max} = 1, x = 0.8$, τ_{PD} denotes the shortest correlation time. The delta function is replaced by a narrow gaussian with width 0.01.

FIG. 2: Calculated EPR lineshapes at $190GHz$ of a nitroxide spin probe for different jump angles ϕ. SCT model (eq.5). Top: from the top to the bottom the correlation time τ_{SCT} is: $6.58 \times 10^{-11}s$; $1.31 \times 10^{-10}s$; $6.58 \times 10^{-10}s$; $1.31 \times 10^{-9}s$; $6.58 \times 10^{-9}s$; $1.31 \times 10^{-8}s$; $6.58 \times 10^{-8}s$. Bottom: from the top to the bottom the correlation time is: $8.33 \times 10^{-11}s$; $1.5 \times 10^{-10}s$; $8.3 \times 10^{-10}s$; $1.66 \times 10^{-9}s$; $2.91 \times 10^{-9}s$; $4.58 \times 10^{-9}s$; $1.0 \times 10^{-8}s$. The magnetic parameters are: $g_x = 2.00994 \pm 3 \cdot 10^{-5}$, $g_y = 2.00628 \pm 3 \cdot 10^{-5}$, $g_z = 2.00212 \pm 3 \cdot 10^{-5}$, $A_x(mT) = 0.62 \pm 0.02$, $A_y(mT) = 0.70 \pm 0.02$, $A_z(mT) = 3.40 \pm 0.02$. The x axis is parallel to the N-O bond, the z axis is parallel to the nitrogen and oxygen $2p$ orbitals containing the unpaired electron, and the y axis is perpendicular to the other ones (see fig.4 for details). Each curve is convoluted with a gaussian with width $0.15mT$. The vertical lines on the top panel mark the positions of the maxima of the outermost peaks at the slowest relaxation rate. They help the reader to appreciate the shifts of the maxima when the reorientation rate increases.

FIG. 3: Dependence of the distance ΔB between the outermost extrema of the HF-EPR lineshape at $190GHz$ (see fig.2) on the rotational correlation time τ for small and large jump angles ϕ.

FIG. 4: Chemical structures of PS and the spin probe TEMPO.

FIG. 5: Temperature dependence of the quantity ΔB at $190GHz$ and $285GHz$ of TEMPO in PS (see fig.2 for the definition). Continuous line: linear fit with $\Delta B_{285} = a + bT$, $a = 44 \pm 0.25mT, b = -0.01394 \pm 0.00123mT\ K^{-1}$. Dashed line: guide for the eye. Inset: average linewidth of the three outermost lines on the right side of the lineshape (see fig.2).

FIG. 6: The line shape at $190GHz$ (a) and $285GHz$ (b) of TEMPO in PS at $50K$. The superimposed dashed lines are best fits according to the SCT model, eq.5, with $\tau_{SCT} = 25ns$ $(190GHz)$ and $\tau_{SCT} = 19ns$ $(285GHz)$. Jump angle $\phi = 60°$. Nearly identical agreement is obtained by decreasing the jump angle down to $\phi = 20°$ with $\tau_{SCT} = 102ns$ $(190GHz)$ and $\tau_{SCT} = 127ns$ $(285GHz)$. Magnetic parameters of TEMPO as in fig.2. The theoretical lineshape is convoluted by a Gaussian with width $0.15mT$ to account for the inhomogeneous broadening.

FIG. 7: The HF-EPR lineshape of TEMPO in PS at $180K$ and frequencies $190GHz$ (a) and $285GHz$ (b). The dotted superimposed lines are simulations by using the SCT model with jump angle $\phi = 20°$ and $\tau_{SCT} = 25.4ns$ (a); $\tau_{SCT} = 29.7ns$ (b). The dashed superimposed line in panel a is a simulation using the SCT model with jump angle $\phi = 35°$ and $\tau_{SCT} = 26.2ns$. Magnetic parameters of TEMPO as in fig.2. The theoretical lineshape is convoluted by a Gaussian with width $0.15mT$ to account for the inhomogeneous broadening.

FIG. 8: The EPR line shape at T=200K and frequencies $190GHz$ (a) and $285GHz$ (b). The dotted lines are numerical simulations by using the TPD model (eq.8 with $\rho = \rho_{PD}$, eq.4) with $x = 0.32$, $\tau_{PD} = 2ns$ (a); $x = 0.28$, $\tau_{PD} = 0.6ns$ (b). For each frequency $\tau_{max} = \tau_{SCT}$ at $180K$ and $\phi = 20°$, see fig.7. From eq.9 the fraction of TEMPO molecules undergoing not activated motion was $w_{190GHz} = 0.44$ and $w_{285GHz} = 0.34$. The dashed lines are numerical simulations by using the SCT model with $\tau_{SCT} = 20.3ns$ (panel a) and $\tau_{SCT} = 21.2ns$ (panel b). In both cases the best fit value of the jump angle is $\phi = 20°$. Notice that TPD model has only *one* more adjustable parameter with respet to SCT one. Magnetic parameters of TEMPO as in fig.2. The theoretical lineshape is convoluted by a Gaussian with width $0.15mT$ to account for the inhomogeneous broadening.

FIG. 9: Temperature dependence of the fraction of trapped TEMPO molecules, eq.9 .

FIG. 10: Best fit of the EPR lineshape using SCT, LGD and PD from 190 GHz, 270 K and a jump angle $\phi = 20°$. For SCT: $\tau_{SCT} = 4.16ns$; for LGD: $\tau_{LGD} = 3.6ns$, $\sigma = 1$; and for PD: $\tau_{PD} = 0.225ns$, $x = 0.575$.Magnetic parameters of TEMPO as in fig.2. The theoretical lineshape is convoluted by a Gaussian with width $0.15mT$ to account for the inhomogeneous broadening.

FIG. 11: Temperature dependence of the width $\overline{E}$ of the exponential energy-barrier distribution, eq.3, as detected by the EPR at $190GHz$ (squares) and $285GHz$ (triangles). Previous measurements by internal friction[31], Raman[18] and light scattering[28] yield $\overline{E}_{IF}/k = 760 \pm 40K$,$\overline{E}_{Raman}/k = 530 \pm 60K$ and $\overline{E}_{LS}/k = 530 \pm 40K$, respectively.

FIG. 12: Temperature dependence of the characteristic times of the SCT, PD and TPD distributions. The error bars at $50K$ and $180K$ account for the uncertainty on the best-fit value of the jump angle which is in the range $20° \leq \phi \leq 60°$, $20° \leq \phi \leq 35°$, respectively . Dotted lines are guides for the eye.

FIG. 13: The exploration of the orientational energy landscape by TEMPO. $T \leq 180K$: all molecules are trapped ($w = 1$). Orientation correlations are lost via non-activated entropic-like pathways. $T > 180K$: a fraction of the molecules equal to $1 - w$ rotate by activated jumps over the exponentially-distributed energy barriers.

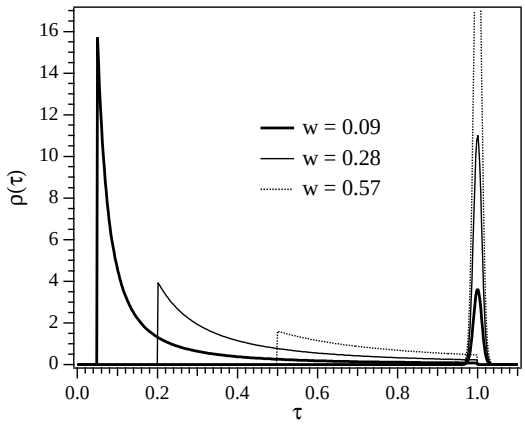

FIGURE 1

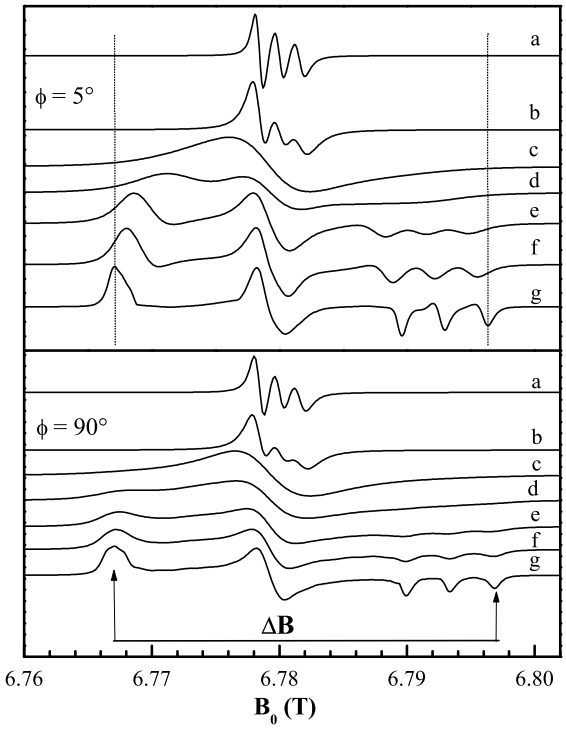

FIGURE 2

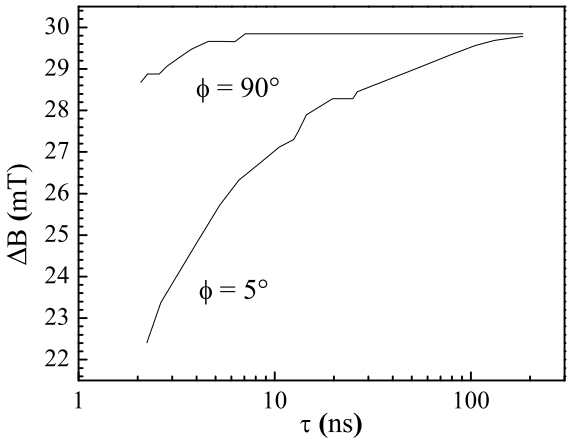

FIGURE 3

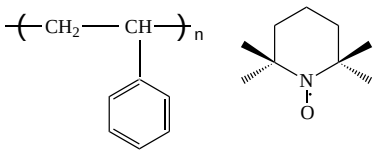

PS TEMPO

FIGURE 4

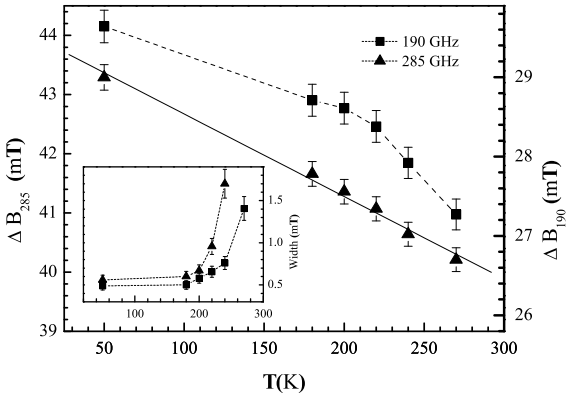

FIGURE 5

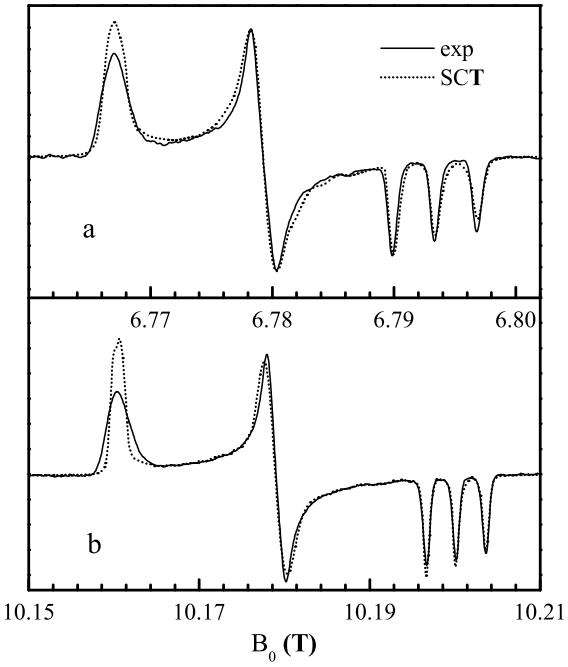

FIGURE 6

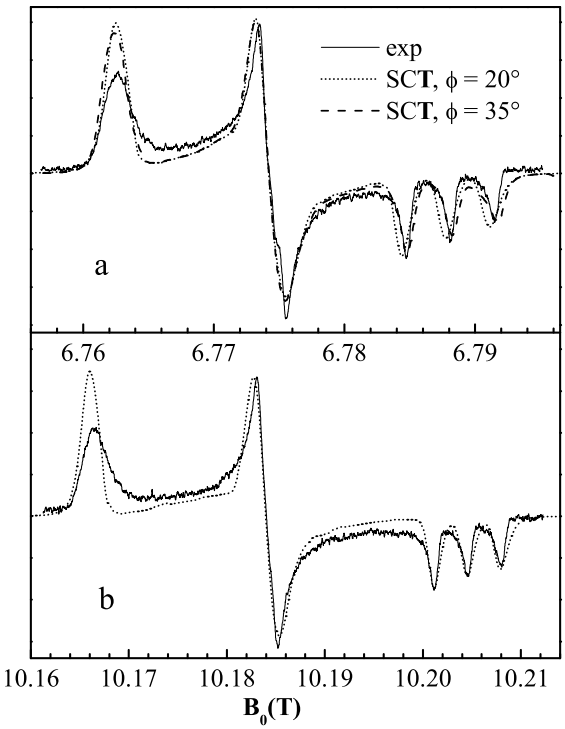
exp
SCT, ϕ = 20°
SCT, ϕ = 35°
a
b
6.76
6.77
6.78
6.79
10.16
10.17
10.18
10.19
10.20
10.21
B0(T)

FIGURE 7

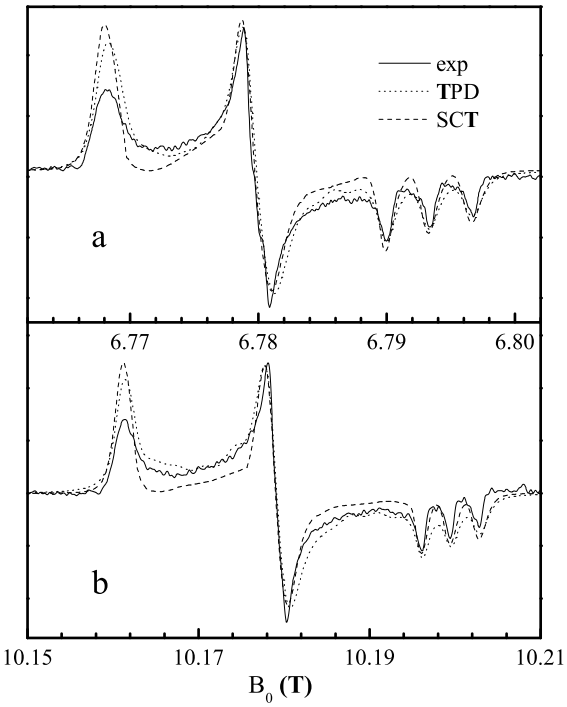

FIGURE 8

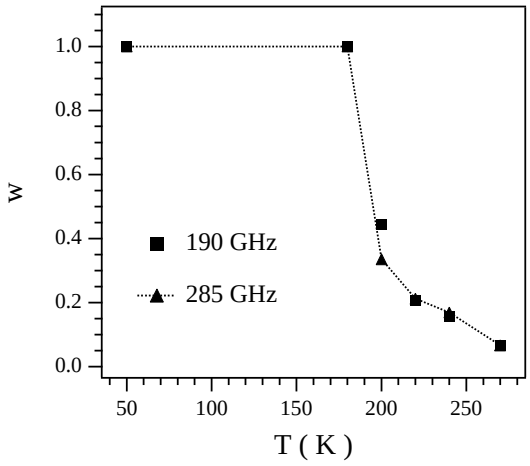

FIGURE 9

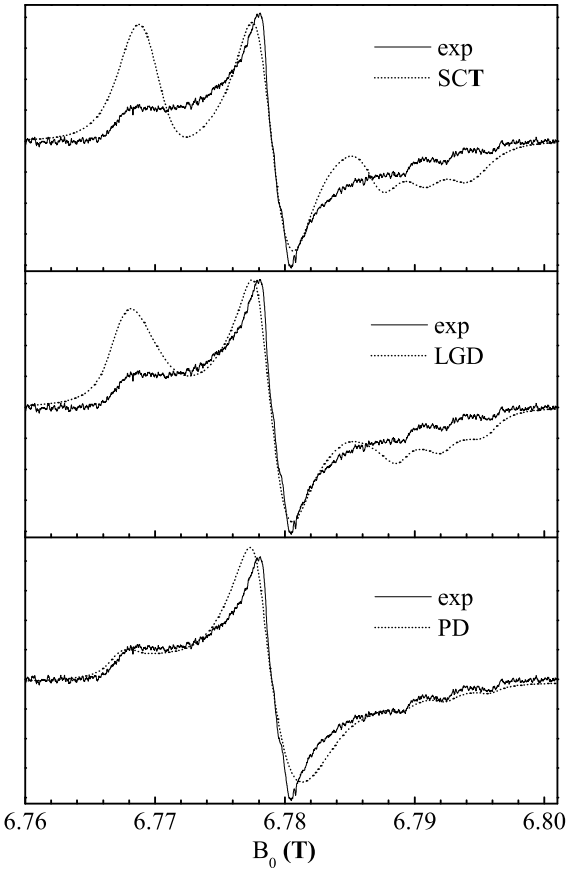

FIGURE 10

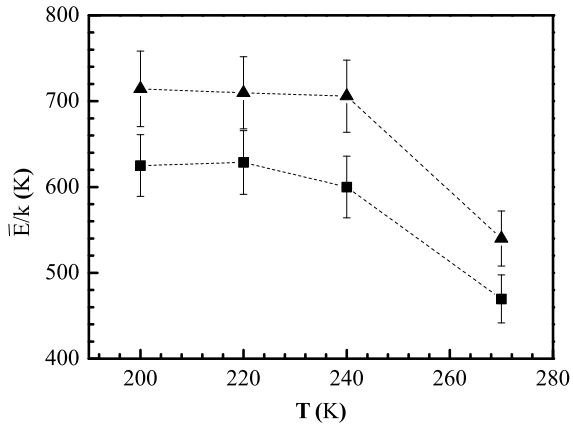

FIGURE 11

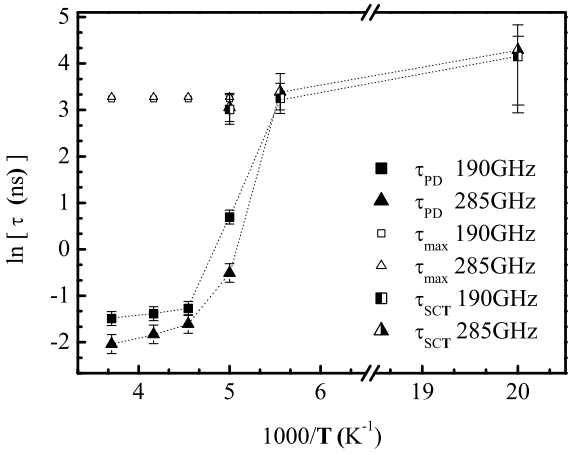
5
4
3
2
1
0
-1
-2
ln [τ (ns)]
4
5
6
19
20
1000/T (K-1)
τPD 190GHz
τPD 285GHz
τmax 190GHz
τmax 285GHz
τSCT 190GHz
τSCT 285GHz

FIGURE 12

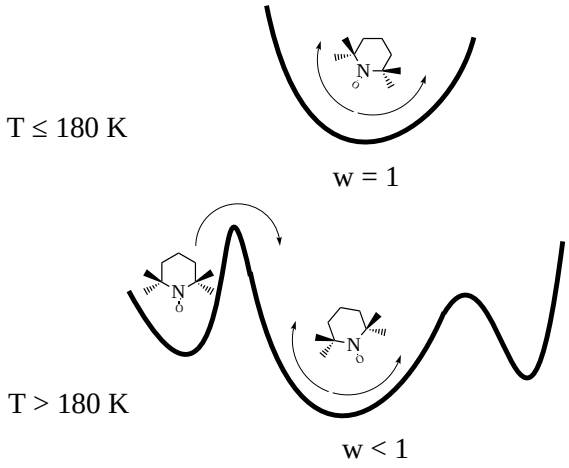

FIGURE 13